Analysis of stress and deformation of a solar PV stand structure under different parameters

Maram A. Zbida
Department of Mechanical and Industrial Engineering,
Faculty of Engineering, University of Tripoli
Tripoli, Libya
Ma.Zbida@uot.edu.ly

Sundus A. Rezg
Department of Mechanical and Industrial Engineering,
Faculty of Engineering, University of Tripoli
Tripoli, Libya
S.Ben_Rezg@uot.edu.ly

Esam Hamza
Department of Mechanical and Industrial Engineering,
Faculty of Engineering, University of Tripoli
Tripoli, Libya
es.hamza@uot.edu.ly

Khaled M. Ahmida
Department of Mechanical and Industrial Engineering,
Faculty of Engineering, University of Tripoli
Tripoli, Libya
k.ashouri@uot.edu.ly

Ahmed Khalifa
Department of Mechanical and Industrial Engineering,
Faculty of Engineering, University of Tripoli
Tripoli, Libya
A.khalifa@uot.edu.ly

Abdussalam A. Ahmed
Mechanical Engineering Department,
Bani Waleed University
Bani Waleed, Libya
abdussalam.a.ahmed@bwu.edu.ly

Abstract**—** As the global energy landscape shifts towards renewable energy sources, photovoltaic (PV) systems are being increasingly deployed. However, their structural stability, particularly under wind loading, remains a key challenge that affects both safety and long-term performance. This study investigates the aerodynamic and structural response of PV panel support systems under various environmental conditions.

Using ANSYS Workbench, several simulation cases were performed, exploring a range of tilt angles (5° to 45°), wind directions (45° to 180°), mounting heights (0.5 m to 3.35 m), and panel sizes. The most critical scenario was identified at a 45° tilt with a 45° wind direction, resulting in the highest levels of stress and deformation. Although such a configuration can maximize solar exposure, it introduces a significant mechanical integrity concern.

In this paper, and to optimize the PV performance in local Libyan climatic conditions, considering a wind direction of 45°, a design featuring a tilt angle of 30°, a mounting height of 2.5 meters, and a medium panel size (2×3 m) was recommended. This configuration achieves a balance between structural integrity and aerodynamic performance. It crucially improves overall system efficiency by minimizing vibrations and deformations, factors that reduce electrical output over time. The study concludes with practical recommendations for the deployment of robust and efficient PV systems in wind-prone areas.

Keywords— solar PV stand; CFD; structural stability; wind loading, stress and deformation, aerodynamic performance

I. Introduction

The interaction between fluid flow and structural systems is a critical area of study in various engineering applications, particularly within the field of renewable energy. Photovoltaic (PV) systems, as a core component of sustainable energy infrastructure, are being increasingly deployed in open outdoor environments where they are continuously exposed to environmental loads. Among these, wind-induced forces represent a significant factor that can compromise the mechanical stability and structural integrity of the supporting frameworks.

These supporting structures are subjected to dynamic forces resulting from unsteady and often turbulent airflow, leading to fluctuating pressure distributions and shear stresses across the surfaces of the PV panels and their mounts. Such forces may induce structural deformations, which over time can culminate in mechanical failure or degradation of performance. Therefore, understanding the behavior of these structures under fluid flow effects, a phenomenon known as Fluid-Structure Interaction (FSI), is essential for optimizing their design and ensuring long-term operational resilience. It highlights key concepts related to fluid dynamics, mechanical stress, and structural deformation, while also offering a critical assessment of the existing literature in the field. Furthermore, it identifies current research gaps that justify the relevance and necessity of this investigation, thereby laying the groundwork for the methodological approach presented in subsequent sections.

The increasing reliance on photovoltaic (PV) solar systems worldwide is a crucial part of global efforts to achieve sustainability and reduce dependence on conventional energy sources. However, environmental loading, particularly wind forces, represents one of the primary challenges that can significantly affect the structural performance and long-term durability of these systems. Solar panels are lightweight structures, often installed in exposed locations, making them highly susceptible to wind effects that generate complex loads on the panel surfaces. This results in uneven pressure distributions, which contribute to excessive stresses that can compromise the stability of the system as a whole.

One of the key factors that has not been adequately studied is the interaction between solar panels and parameters like wind speed, wind direction, tilt angle, and panel height. This interaction is crucial to understanding the structural behavior of solar panels under various environmental conditions, as these factors intersect to affect the distribution of aerodynamic loads and the resulting stresses. Additionally, the impact of different panel sizes has not been explored adequately, meaning that a significant gap in the knowledge of how these factors influence the structural response of PV systems.

The problem addressed in this study lies in the need to develop an integrated simulation framework that employs advanced techniques such as computational fluid dynamics (CFD) and static structural analysis, to assess the combined effects of wind speed, wind direction, tilt angle, and panel geometry on stresses and deformations in solar panels. Addressing this research gap is critical for enhancing the design of solar panels and ensuring their structural efficiency and long-term performance studies have addressed the impact of wind on solar panels, most of these studies have focused on analyzing the effect of individual variables such as tilt angle, wind speed, or wind direction in isolation, without considering the intricate interactions between these factors. Several studies have investigated the aerodynamic behavior of solar panels using both numerical and experimental methods.

Shademan and Hangan [1] conducted three-dimensional CFD simulations using the RANS model with k−ω SST turbulence modeling. Their study examined the impact of seven wind directions on a solar panel with a fixed tilt angle of 45° and a wind speed of 90 km/h. The results showed maximum wind loads at 0° and 180°, with the bottom panels experiencing higher forces. The presence of panel gaps was found to influence airflow and generate additional vortices.

Mohaptra [2] carried out an experimental study of the wind tunnel under similar conditions. Their findings confirmed the simulation results by Shademan and Hangan [1], particularly the location of peak wind loading, thereby validating the numerical approach.

Darhouane [3] expanded on these findings by analyzing three tilt angles (15°, 25°, 45°) and four wind directions (0°, 45°, 135°, 180°). Larger panel dimensions were used, which affected the load distribution. This study highlighted the amplified wind forces at higher tilt angles and added insight into more optimal tilt configurations. His results also aligned with those of Jubayer et al. [4], who conducted experimental wind tunnel tests in similar settings.

Kumar and Prakash [5] conducted a CFD-based study to evaluate the aerodynamic performance of solar panels at different tilt angles (30°, 45°, and 60°) under steady-state wind flow conditions. The simulations were carried out using ANSYS Fluent to understand the pressure distribution and force behavior. The results showed that the maximum drag force occurred at 60° tilt, while the maximum lift force was observed at 45°, helping to identify an optimal configuration for solar panel installation.

Yemenici [6] conducted a numerical investigation to evaluate the effect of wind direction on the aerodynamic performance of a ground-mounted solar panel. The study used a constant wind speed of 10 m/s and a fixed tilt angle of 25°, with wind directions varied at 0°, 45°, 135°, and 180°. The results showed that the highest-pressure coefficients appeared at the leading edge for all cases, decreasing toward the trailing edge. The maximum drag was observed at 0° wind direction, while the minimum occurred at 135°. The lift coefficients were found to be negative for 0° and 45°, and positive for 135° and 180°, highlighting the directional sensitivity of the aerodynamic forces on the panel.

Apparao [7] conducted a CFD-based study to optimize the structural orientation of pole-mounted solar panels under high wind loads. Simulations were performed for wind speeds of 55 m/s and 70 m/s at inclination angles of 28°, 30°, 32°, and 34°. The results indicated that a 32° tilt angle minimizes both the drag coefficient and the turbulent kinetic energy, making it the most aerodynamically favorable orientation. The corresponding dynamic pressure was applied to a static structural model of the pole mount, and the resulting Von Mises stress and total deformation remained within safe limits (below the yield strength of structural steel). The study concluded that a 32° inclination provides a structurally safe and aerodynamically efficient configuration under high wind conditions.

Baetu et al. [8] conducted a numerical simulation using ANSYS CFX 12 to investigate wind effects on an array of 12 ground-mounted solar panels tilted at 30°. The study explored five different wind directions: 0°, 30°, 45°, 135°, and 180°. The results highlighted that wind direction plays a crucial role in the pressure distribution across the panel array. Specifically, higher suction pressures were observed at 30°, 45°, 60°, and 135°, attributed to the formation of conical vortices due to oblique wind incidence. The highest suction occurred in a wind direction of 45°, making it the most critical case in terms of aerodynamic loading on the array.

This study primarily aims to integrate the Computational Fluid Dynamics (CFD) with static structural analysis to assess the deformations and mechanical stresses resulting in a solar PV stand structure under different conditions, thereby enhancing the design of solar panels and ensuring their structural integrity and long-term durability.

II. GOVERNING EQUATIONS

To simulate air flow around the photovoltaic panel, the governing equations of incompressible fluid flow were applied. These include the following:

- the continuity equation, which ensures mass conservation
- conservation of mass $div(\rho u) = 0$

The momentum equation, which represents the conservation of momentum:

X-momentum equation:

$$\rho\left(u\frac{\partial u}{\partial x} + v\frac{\delta u}{\delta z} + w\frac{\delta u}{\delta z}\right) = \rho g_x - \frac{\partial p}{\partial x} + \mu\left(\frac{\partial^2 u}{\partial x^2} + \frac{\partial^2 u}{\partial y^2} + \frac{\partial^2 u}{\partial z^2}\right) \qquad (1)$$

Y-momentum equation:

$$\rho\left(u\frac{\partial u}{\partial x} + v\frac{\delta u}{\delta z} + w\frac{\delta u}{\delta z}\right) = \rho g_y - \frac{\partial p}{\partial y} + \mu\left(\frac{\partial^2 v}{\partial x^2} + \frac{\partial^2 v}{\partial y^2} + \frac{\partial^2 v}{\partial z^2}\right) \qquad (2)$$

Z-momentum equation:

$$\rho\left(u\frac{\partial u}{\partial x} + v\frac{\delta u}{\delta z} + w\frac{\delta u}{\delta z}\right) = \rho g_z - \frac{\partial p}{\partial z} + \mu\left(\frac{\partial^2 w}{\partial x^2} + \frac{\partial^2 w}{\partial y^2} + \frac{\partial^2 w}{\partial z^2}\right) \qquad (3)$$

These equations form the basis for the Navier–Stokes formulation used in CFD simulations. To model the turbulence, the k–ω SST turbulence model was used. It combines the advantages of the k–ε model in the far field with the k–ω model near the walls. This hybrid approach improves the prediction of flow separation and wall-bounded behavior, which is essential for accurately estimating aerodynamic loads on the solar panel.

The Menter SST (shear stress transport) k–ω turbulence model combines the advantages of the k–ω model near walls and the k–ε model in the free-stream through a blending function. This model is widely used in aerodynamic simulations due to its ability to accurately predict boundary layer separation and near-wall flow behavior. The model is governed by two transport equations: one for the turbulent kinetic energy (k) and one for the specific dissipation rate (ω). These equations are expressed as:

$$\left(\frac{\partial}{\partial t}(\rho k) + \frac{\delta}{\delta x}(\rho k u_i)\right) = \frac{\partial}{\partial x_j}\left(\Gamma_k \frac{\partial k}{\partial x_j}\right) + G_k - Y_k + S_k \qquad (4)$$

$$\left(\frac{\partial}{\partial t}(\rho \omega) + \frac{\delta}{\delta x_j}(\rho \omega u_j)\right) = \frac{\partial}{\partial x_j}\left(\Gamma_\omega \frac{\partial \omega}{\partial x_j}\right) + G_\omega - Y_\omega + D_\omega + S_\omega \qquad (5)$$

The von Mises stress is an equivalent or effective stress at which yielding is predicted to occur in ductile materials. von Mises stress is given using principal axes in terms of the principal stresses σ1, σ2, and σ3 as

$$\sigma' = \frac{1}{\sqrt{2}}\left[\left((\sigma 1 - \sigma 2)^2 + (\sigma 1 - \sigma 3)^2 + (\sigma 2 - \sigma 3)^2\right)\right]^{\frac{1}{2}} \qquad (6)$$

Nonetheless, there might be normal and shear stresses present at many sites in the material that are under static or dynamic loads. Therefore, the state of stress can also be stated in terms of the normal stresses σ_x, σy, and σ_z, and the shear stresses τ_{xy}, τ_{yz}, and τ_{zx}, where the coordinate axes are non-principal axes. The von misses stress with respect to non-principal axes is given below**.**

$$\sigma' = [(((\sigma x - \sigma y)^2 + (\sigma y - \sigma z)^2 + (\sigma z - \sigma x)^2) + 6((\tau xy)^2 - (\tau xy)^2 + (\tau xy)^2)]^{\frac{1}{2}} \qquad (7)$$

III. NUMERICAL MODEL

A. *Description of Geometry, Meshing and Investigated Parameters*

A three-dimensional model was created to study the effect of aerodynamic loads based on the model presented by Shademan and Hangan [1], which in turn was based on experimental data published by Mohapatra [2]. This model represents a single photovoltaic panel mounted on a ground structure and exposed to wind in an open environment. It is considered the baseline case on which all subsequent analyzes are based. The panel is represented with dimensions of 4.3 x 3.2 m, an angle of inclination of 45 degrees, and a height of 3.35 m above sea level.

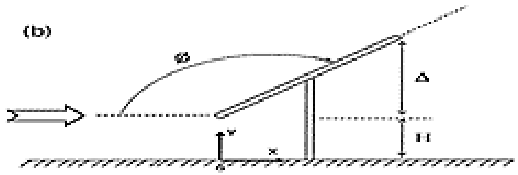

Fig 1. A Photovoltaic panel mounted on a ground structure.

In order to evaluate the different installation conditions on the aerodynamic and structural response of the photovoltaic panel support structure, a parametric study was adopted that included four main variables. These variables represent a wide range of realistic operating conditions and were designed so that each variable change individually while the rest of the factors remain fixed at their values. reference values, the following parametric variables were included:

Angle of inclination: Four installation angles were analyzed: 5, 15, 30, and 45. This was done to evaluate how changes in the angle of inclination affect the pressure distribution and aerodynamic analysis. The angles were measured from the horizontal position of the surface.

Wind direction: Airflow was simulated at four relative angles: 45, 90, 135, and 180. This was done to represent the effect of changes in wind direction on the dynamic response of the board.

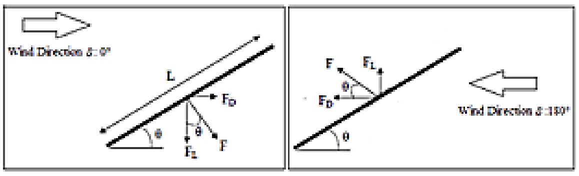

Fig 2. The effect of changes in wind direction on the loads.

Installation height: The analysis included four height levels: 0.5m, 1.5m, 2.5m, and 3.35m; in order to evaluate the effect of board height on pressure distribution and wind load.

Panel area: Four board sizes 4.2x3.2 3x2 2x1 1x0.7were studied to investigate how the area exposed to wind affects aerodynamic and structural dynamic responses.

The numerical simulations for this study were performed using ANSYS Workbench, which integrates both the Fluent module for Computational Fluid Dynamics (CFD) analysis and the Static Structural module for static structural analysis. The initial model was created using SolidWorks software due to its flexibility in three-dimensional mechanical design. Then it was imported into ANSYS software to setup the air flow domain, generate the mesh, and apply the required boundary conditions.

The study initially focused on performing a complete computational fluid dynamics (CFD) analysis, where the aerodynamic forces acting on the solar panel, including the drag and lift forces, were calculated. Performance coefficients such as the drag coefficient (CD) and the lift coefficient (CL) were also extracted. The surface pressure distribution resulting from the CFD analysis was then exported to the solid structure module within ANSYS to perform a one-way coupling to analyze the structural effects resulting from aerodynamic loads, including the distribution of normal stresses, shear stresses, and von Mises stresses.

The panel was placed in a three-dimensional computational domain measuring 100 meters long, 46 meters wide, and 20 meters high. This domain was chosen to minimize the impact of the side and top boundaries on the flow field, with a distance of 20 meters from the panel to the inlet, allowing the wind patterns to fully form before interacting with the structure.

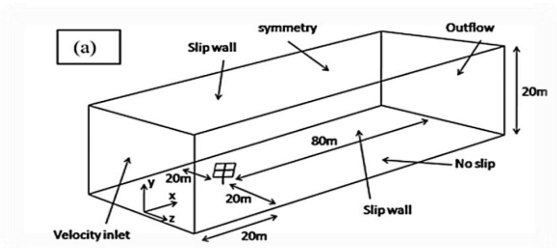

Fig 3. Domain dimensions and boundary conditions.

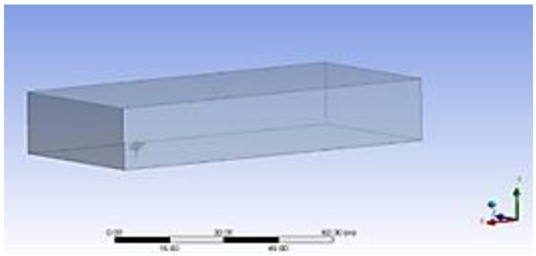

Fig 4. Domain dimensions and boundary conditions from the simulation by ANSYS.

A standard wind speed of 25 meters per second was set at the entrance based on the recommendations of ASCE-7-05 for open convergence conditions.

A hybrid mesh consisting of tetrahedral (Tet) and hexahedral (Hex) elements was used. The mesh was automatically generated using ANSYS meshing tools, with further refinements in areas of strategic importance. A local refinement box was included around the solar panel to increase mesh accuracy near high-gradient areas, such as wind-facing surfaces and areas prone to flow separation where aerodynamic forces are more sensitive to geometric and flow changes. Overall, grid quality metrics confirmed a well-optimized grid suitable for capturing both aerodynamic and structural responses with high confidence. Particular attention was paid to the near-wall region to ensure the accuracy of the viscous sublayer effect. Based on the recommendations of Shademan and Hangan [1], the non-dimensional wall distance y^+ (also referred to as h^+) was kept below 1 in all simulations:

$$y^+ = \frac{\rho . u_t . y}{\mu} \quad (8)$$

where u_t is the friction velocity, y is the distance from the wall to the center of the first computational cell, ρ is the fluid density, and μ is the dynamic viscosity. This ensures that the grid accurately captures the laminar sublayer, which is necessary for modeling the low Reynolds numbers (LRNM) used in this paper. This modeling approach avoids the use of wall functions and provides a more detailed representation of the turbulent flows surrounding the wall. To ensure that the numerical results are independent of mesh resolution, a mesh independence study was conducted. Several mesh configurations with an increasing number of elements were tested, and aerodynamic responses, particularly the drag force, were monitored. The results showed little variation beyond a mesh size of approximately 2.6 million elements, confirming the mesh independence. Consequently, a final mesh consisting of approximately 2.6×10^6 elements was adopted for all basic and parametric cases, achieving a balance between computational efficiency and solution accuracy.

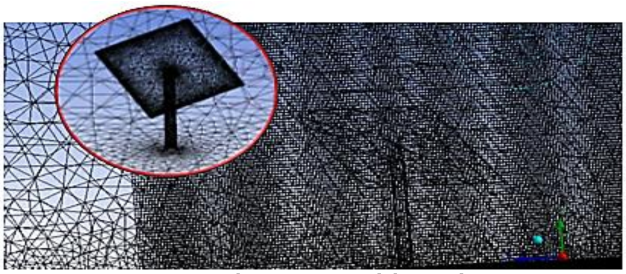

Fig 5. Mesh structur around the panels.

A mesh independence study was conducted where several grids with element count ranging from 800,613 to 4,274,106 were tested at an angle of attack of 30 degrees. The results showed stability in the drag coefficient (CD) and lift coefficient (CL) values at approximately 2.6 million elements, with a relative change of less than 1%.

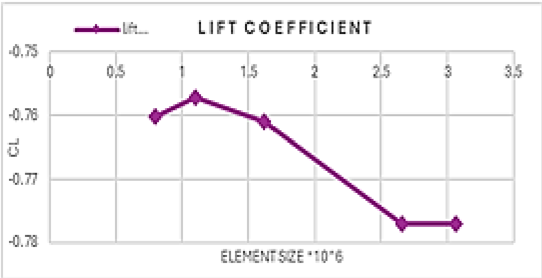

Fig 6. Lift coeffecient (mesh independent study).

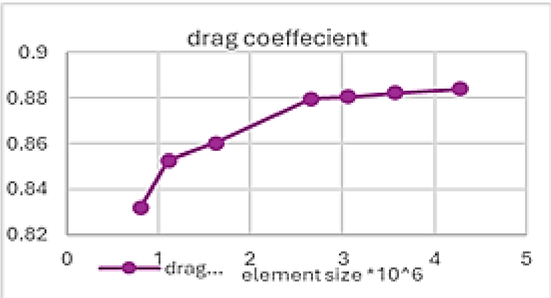

Fig 7. Drag coeffecient (mesh independent study).

B. Boundary Conditions

The inlet boundary was defined as a velocity inlet with a constant wind speed of 25 m/s, representing a reference wind speed for open terrain conditions. The outlet boundary was defined as a pressure outlet with a pressure measurement of 0 Pa, allowing air to flow out of the domain without numerical reflections. The ground surface and the solar panel were treated as wall boundaries with no slip conditions, which means that the velocity on the surface is zero to correctly capture near-wall viscous effects. The top and side boundaries were set as matching conditions to minimize boundary effects and simulate an open atmosphere.

The effects of turbulence were modeled using the k-ω SST turbulence model, which provides high accuracy in capturing near-wall behavior and flow separation regions. The simulation was carried out under steady-state conditions using the SIMPLE algorithm for pressure and velocity coupling. The convergence was monitored through the residuals of velocity, pressure, and turbulence quantities, with the convergence criterion set to 10-6, ensuring stable and accurate results.

IV. Simulation Scenarios

All scenarios in the simulation were based on the baseline, which represents a photovoltaic panel mounted on a structure at an angle of 45 degrees and an installation height of 3. Wind speed was 25 meters per second. The simulation was performed using the One-Factor-At-a-Time (OFAT) methodology, i.e., changing one variable while keeping the other factors at their reference values. This method allows isolating the individual effect of each variable on the wind forces and the structural response of the structure. The study included four main groups of scenarios.

Angle of inclination: Four different inclination angles of 5 degrees 15 degrees, 30 degrees, and 50 degrees were analyzed to evaluate how changes in the inclination of the panel affect pressure distribution and the aerodynamic load. The angles were measured from a flat horizontal position.

Wind direction: Wind approach angles of 45^o, 90^o, 135^o, and 180^o were analyzed to understand the effect of wind direction on force magnitudes and stress patterns across the panel.

Panel surface area: Four different panel sizes were modeled: 4.2 × 3.2 m, 2 × 3 m, 1 × 2 m, and 0.7 × 1 m, to study how the total area exposed to wind affects aerodynamic and structural responses. Height: The height of the panels above ground level was varied across four levels: 0.5 m, 1.5 m, 2.5 m, and 3.35 m, to capture the effect of height within the atmospheric boundary layer on wind interaction. Thirteen simulation cases were performed, representing different combinations of the above parameters. In each case, the remaining variables were fixed at their default values to isolate the effect of the specific variable under study. All simulations were performed using the same numerical setup, coupling strategy, and boundary conditions used in the approved baseline model, ensuring consistency and comparability between cases.

This parametric study provides valuable information on the behavior of solar panel structures under various operating conditions, providing a solid foundation for improving design practices that aim to enhance structural stability and aerodynamic efficiency.

The structural analysis was the next step after the aerodynamic analysis, using the CFD simulation results as input loads for the structural model. This was achieved by adopting a one-way coupling, where the surface pressure fields calculated from Fluent were transferred directly to Static Structural. The structural analysis included pressure analysis, stress calculation, and deformation assessment.

This model assumed that the supporting structure was made of aluminum alloy due to its suitable properties, light weight, and corrosion resistance. As for the boundary conditions, the ground bases were fixed using fixed support conditions to simulate actual installation.

V. Validation of the Numerical Model

To verify the reliability of the model, a comparison was made with the results reported by Shademan and Hangan [1], which in turn refer to the experimental measurement results reported by Mohaptra [2]. The verification was performed using lift and drag coefficients, with a focus on the drag coefficient and its variation with wind direction. Good agreement was found with the reference values, with a slight deviation. The verification process also included a qualitative comparison of the surface pressure distribution along the panel, which further confirmed the model's ability to replicate the main aerodynamic behaviors observed in physical experiments[9,10,11].

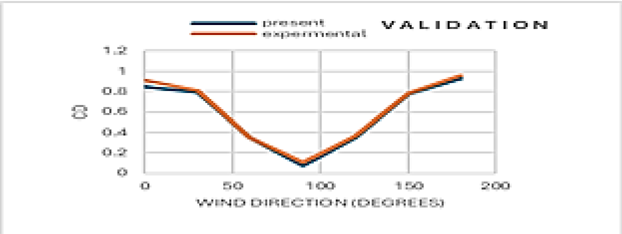

Fig 8. Comparison of CFD and experiments obtained CD versus wind direction.

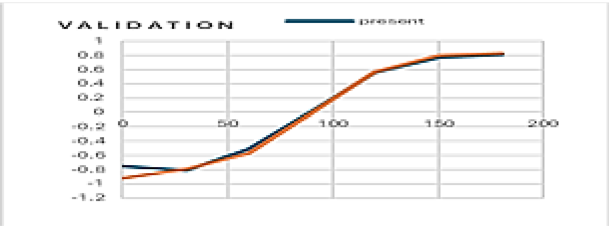

Fig 9. Comparison of CFD and experiments obtained CL versus wind direction.

VI. Results for Stand-Alone Panels

A. Tilt Angle Effect

The numerical simulation results revealed that the drag coefficient (CD) increases progressively with the rise in tilt angle. This is attributed to the increasing frontal area exposed to wind flow. At lower tilt angles, such as 5°, the surface area facing the oncoming wind is relatively small, resulting in lower aerodynamic resistance. In contrast, at higher tilt angles, such as 45°, the panel becomes more perpendicular to the wind, significantly increasing the drag force and, consequently, the CD value.

Regarding the lift coefficient (CL), all examined cases exhibited negative values. This indicates that the vertical aerodynamic forces generated by the wind action are directed downward, pressing against the panel surface rather than lifting it. The magnitude of this downward force increases with the tilt angle. At 5°, the CL value is close to zero, but it becomes increasingly negative as the tilt angle increases, with the most pronounced negative value observed at 45°. This behavior can be explained by the pressure distribution on the panel surfaces, where the lower surface experiences higher pressure than the upper surface, thus generating a negative lift force.

These findings suggest that increasing the tilt angle not only intensifies the drag forces but also imposes a greater downward pressure on the panel. Such effects must be carefully considered when designing the structural support systems of solar panel installations.

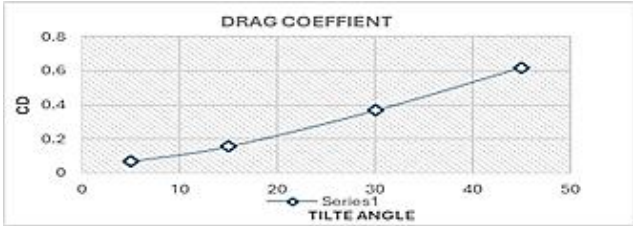

Fig 10. Drag coefficient v/s tilt angle.

Fig 11. Lift coefficient v/s tilt angle.

The pressure distribution on the panel at the tilt angels of (a) θ=5°, (b) θ=15°, (c) θ=30°, and (d) θ=45°, are all shown in Fig. 12.

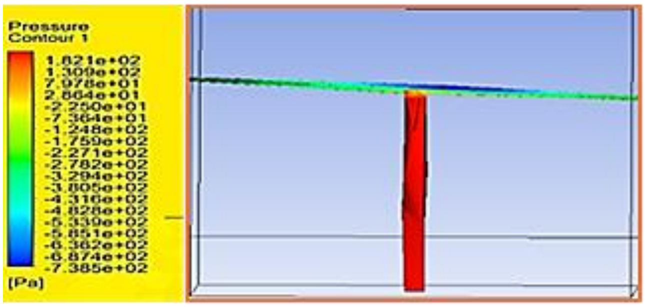

(a)

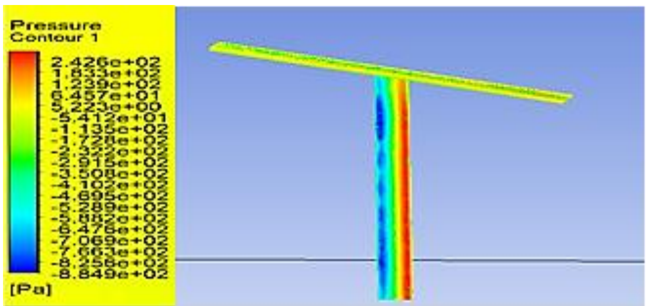

(b)

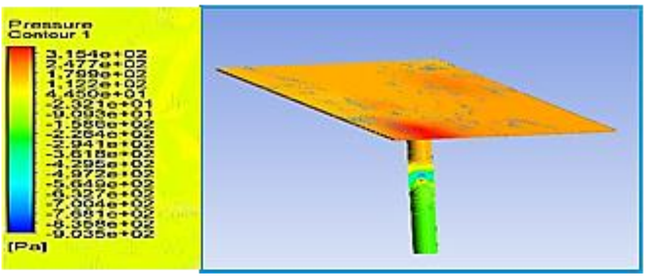

(c)

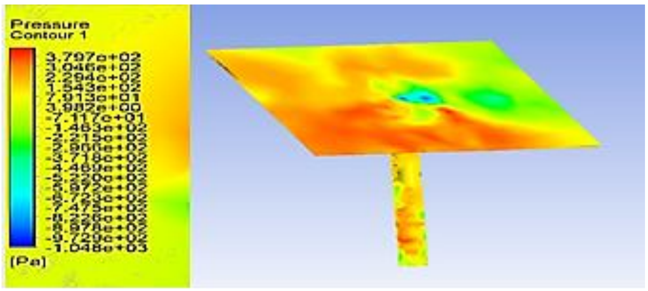

(d)

Fig 12. Pressure distribution for tilt angels of θ= 5°, 15°, 30°, and 45°.

The velocity contours on the panel at the same tilt angles of (a) θ=5°, (b) θ=15°, (c) θ=30°, and (d) θ=45°, are all shown in Fig. 13.

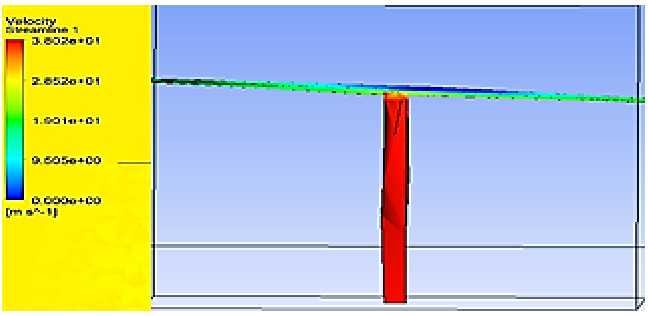

(a)

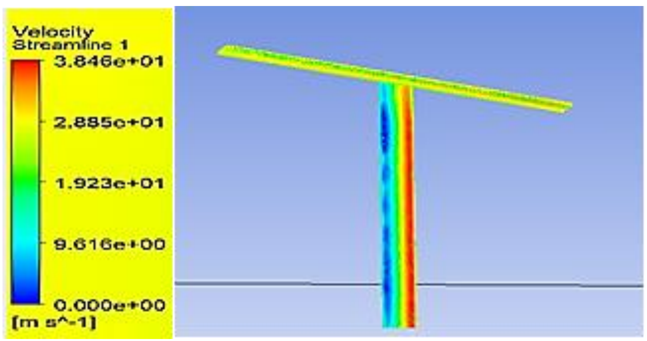

(b)

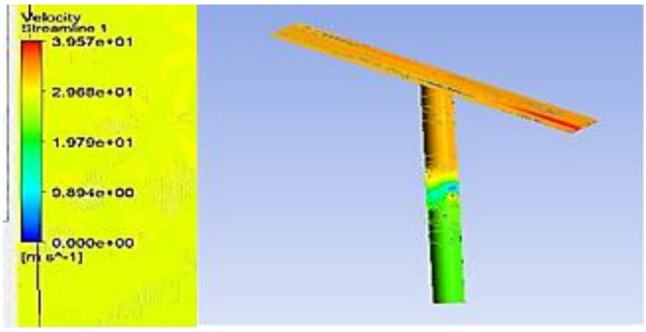

(c)

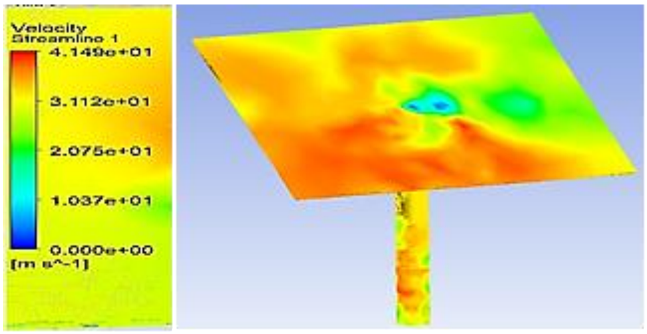

(d)

Fig 13. Velocity distribution for the tilt angels of θ= 5°, 15°, 30°, and 45°.

From a structural point of view, the deformation and stress values showed a clear upward trend with increasing tilt angles. Maximum responses were observed at a 45° tilt, suggesting that such configurations impose significant mechanical loads, which may affect the long-term durability and safety of the mounting system—especially in regions with high wind speeds.

The static structural contours at a tilt angle of 45° are calculated and demonstrated in Fig. 14. In this figure, the total deformation, the normal stress, the equivalent (von Mises) stress, and the shear stress are shown.

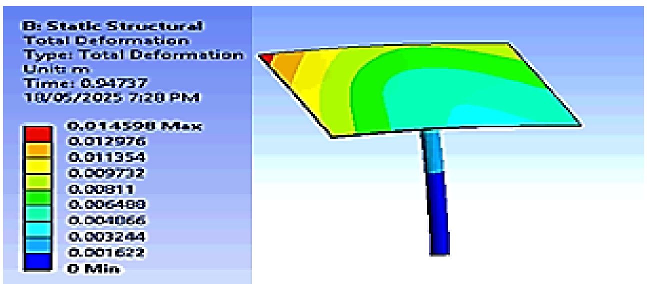

(a) total deformation

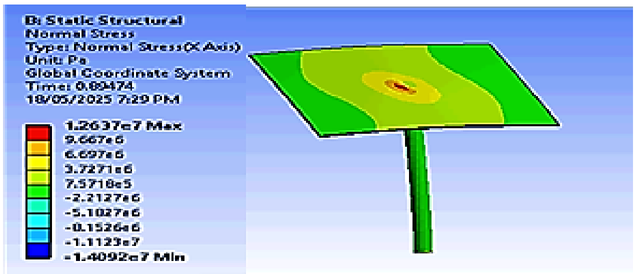

(b) normal stress

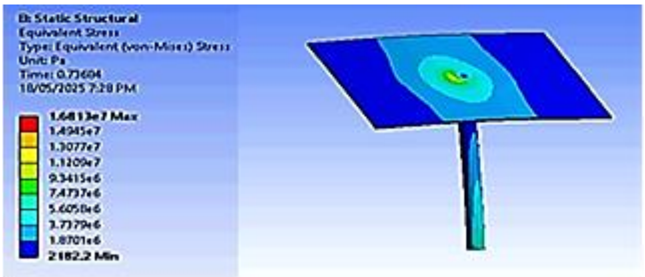

(c) equivalent stress

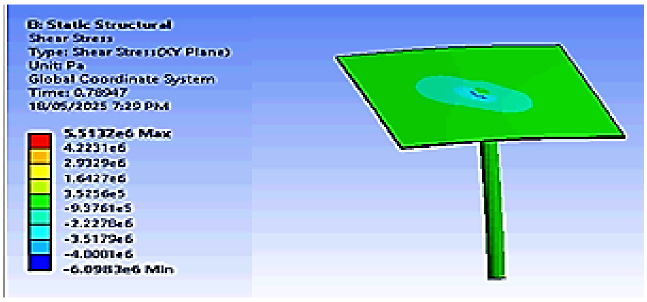

(d) shear stress

Fig 14. Static structural contours at 45° tilt angel: (a) total deformations, (b) normal stress, (c) equivalent (von-Mises) stress, and (d) shear stress.

B. *Wind Direction Effect*

Conducting an aerodynamic analysis, the results showed a clear variation in the drag coefficient (CD) and the lift coefficient (CL) with changing wind direction, as shown in Fig. 15. The highest CD value occurred at 180° followed by 135° ,45°, and the lowest at 90° This indicates that rear-facing wind (180°) creates a large low-pressure region behind the panel, resulting in a high drag force. On the contrary, at 90°, the wind flows along the panel side with minimal direct impact, producing the least resistance.

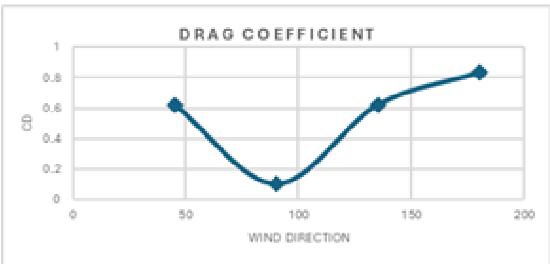

Fig 15. Drag coefficient change against wind direction.

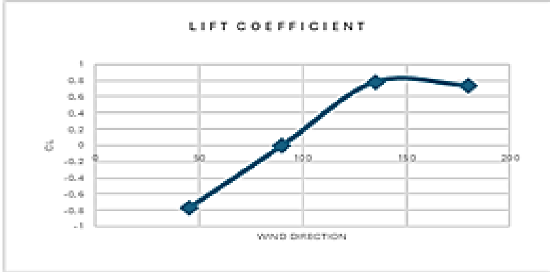

Fig 16. Lift coefficient v/s wind direction.

The pressure distribution on the panel structure is analyzed for different wind directions of: (a) θ=45°, (b) θ=90°, (c) θ=135°, and (d) θ=180°, as demonstrated in Fig. 17.

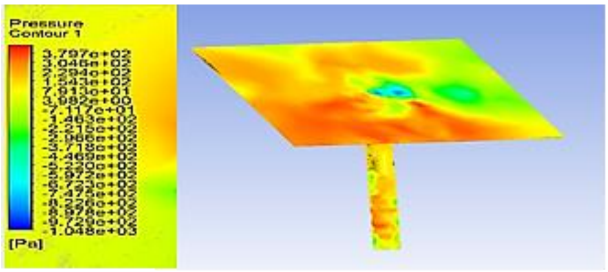

(a) wind direction of 45°.

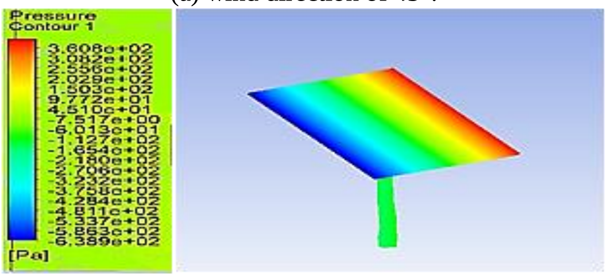

(b) wind direction of 90°.

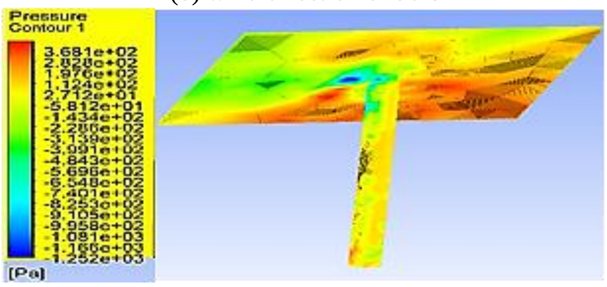

(c) wind direction of 135°.

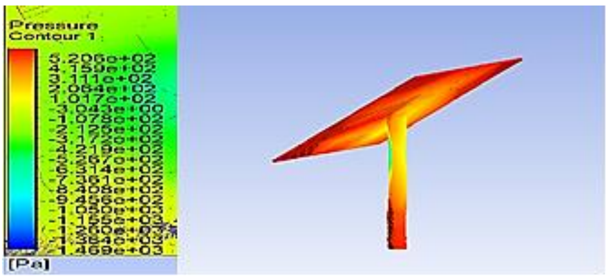

(d) wind direction of 180°.

Fig 17. Pressure distribution of structure for different wind directions.

The velocity distribution on the panel structure is also analyzed for different wind directions of: (a) θ=45°, (b) θ=90°, (c) θ=135°, and (d) θ=180°, as demonstrated in Fig. 17.

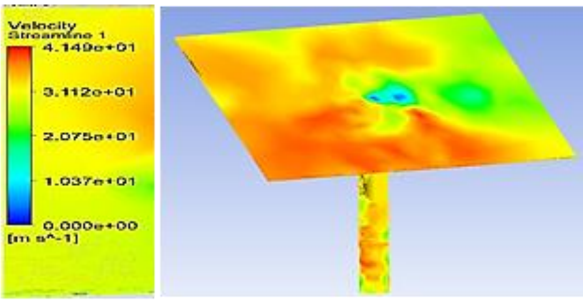

(a) wind direction of 45°.

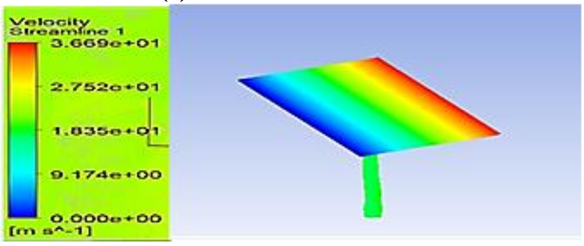

(b) wind direction of 90°.

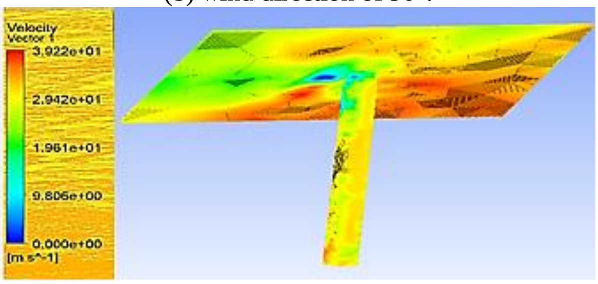

(c) wind direction of 135°.

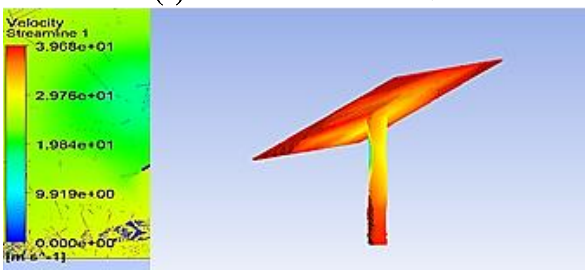

(d) wind direction of 180°.

Fig 18. Velocity distribution of structure for different wind directions.

Regarding the lift coefficient (CL), the values were positive at 135° and 180°, indicating an upward lift due to pressure differences across the panel surfaces. Conversely, CL values were negative at 45° and 90°, signifying a downward force caused by higher pressure on the front-facing surface. These shifts in CL reflect the changing pressure distribution around the panel as the wind direction changes.

Structural analysis revealed that the highest values of von Mises stress, normal stress, and deformation occurred at 45°. This is attributed to the oblique wind direction generating a combined load with both vertical and horizontal components, producing a more complex and severe impact on the structure, especially near the panel edges and corners. Although the highest drag coefficient was observed at 180°, its structural effect was relatively lower than at 45°, since the force acts more perpendicularly and with less torsional influence.

For the sake of comparison, the static structural contours is again analyzed at a tilt angle of 90°. The obtained contours are as demonstrated in Fig. 19. In this figure, the total deformation, the normal stress, the equivalent (von Mises) stress, and the shear stress are shown.

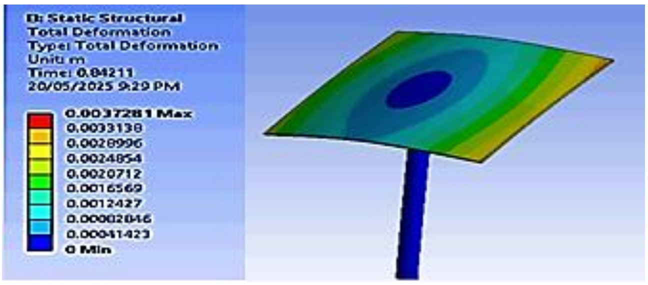

(a) total deformation

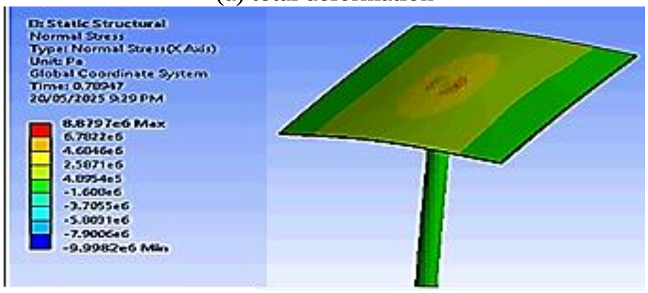

(b) normal stress

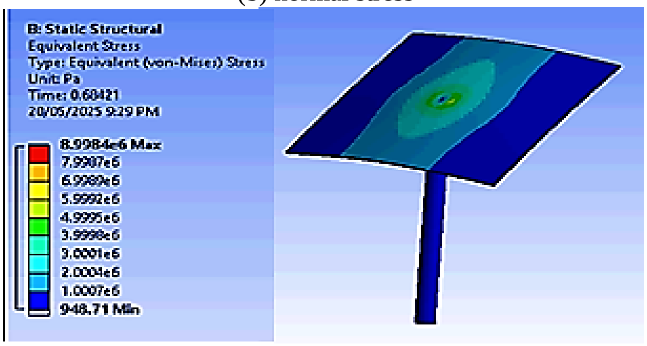

(c) equivalent stress

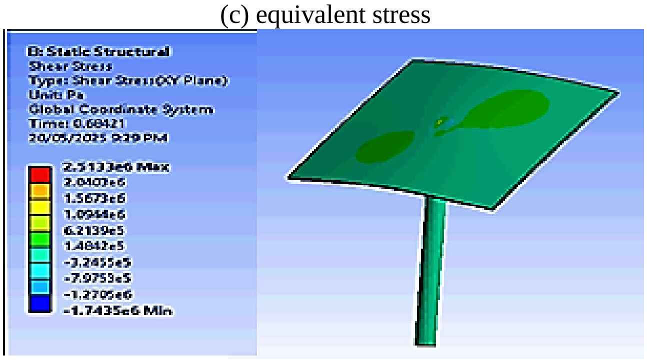

(d) shear stress

Fig 19. Static structural contours at 90° tilt angel.

This finding highlights the importance of evaluating the overall structural response rather than relying solely on aerodynamic parameters such as CD, as the resulting impact depends both on the magnitude and orientation of the acting forces.

C. Mounting Height Effect

From an aerodynamic behavior point of view, the CFD results revealed a clear trend of increasing the drag coefficient (CD) and lift coefficient (CL), along with their corresponding forces (F_D and F_L), as the mounting height increased. These behaviors are shown in Fig. 20 and Fig. 21, respectively. These are attributed to the panels being exposed to a higher-speed, less turbulent airflow at greater elevations, away from the influence of the near-ground boundary layer. Consequently, the aerodynamic loading on the panels' surfaces intensifies with height.

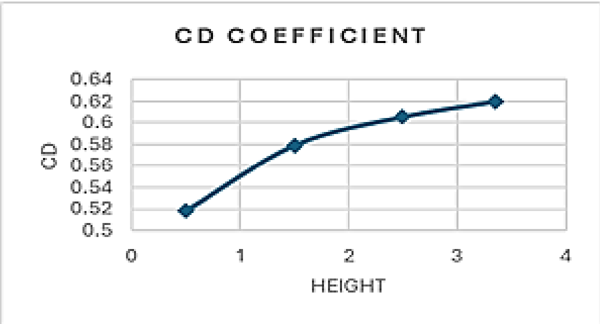

Fig 20. Drag coefficient v/s Height.

Fig 21. Lift coefficient versus height change.

The change in pressure distribution at these mounting heights of: (a) H=0.5m, (b) H=1.5m, (c) H=2.5m, and (d) H=3.35m is as illustrated in Fig. 22.

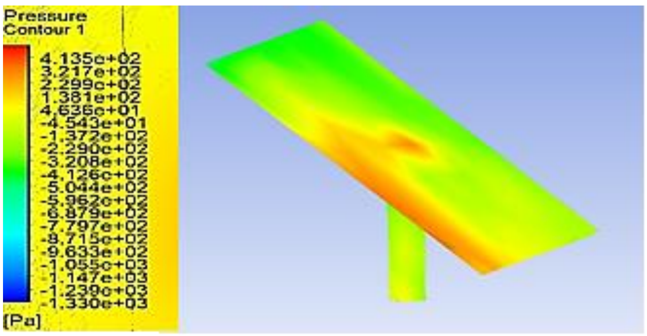

(a) H=0.5m

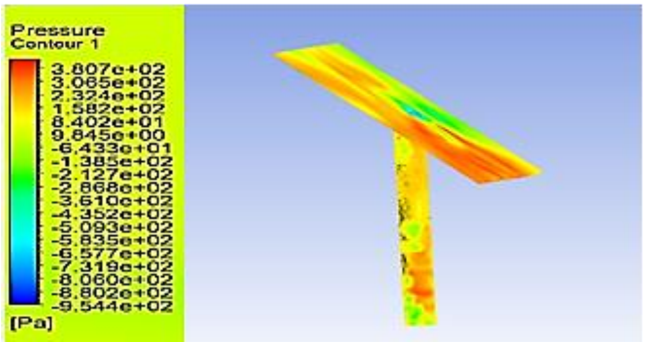

(b) H=1.5m

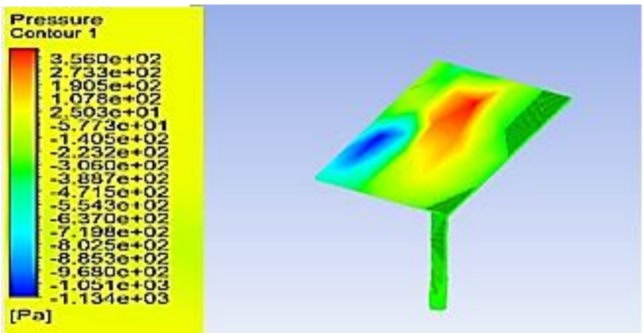

(c) H=2.5m

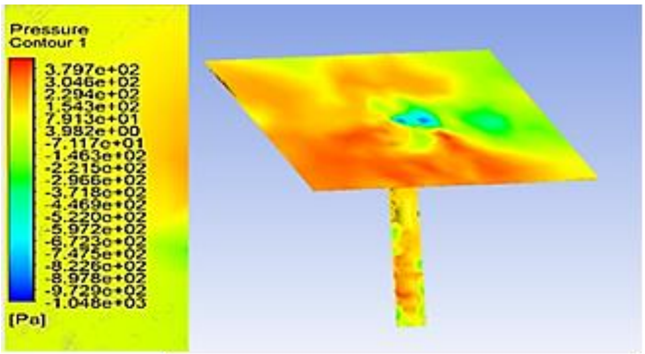

(d) H=3.35m

Fig 22. Pressure distribution for different heights of panel.

The change in velocity distribution at varying mounting heights is as illustrated in Fig. 23.

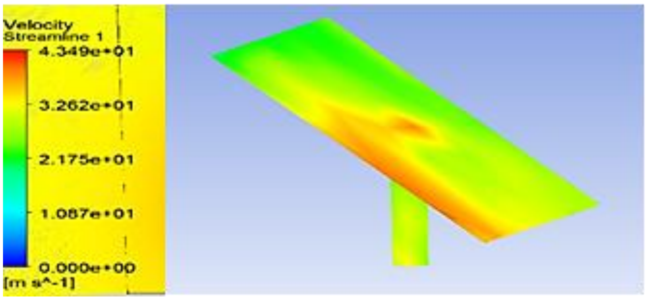

(a) H=1.5m

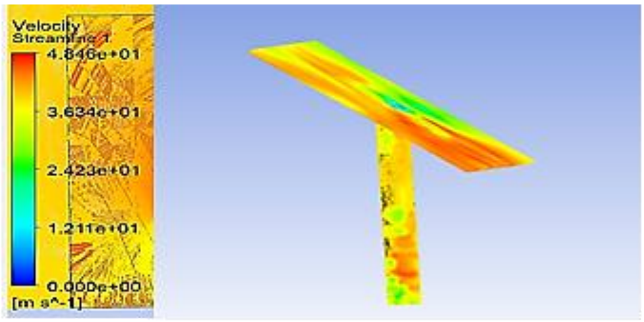

(b) H=2.5m

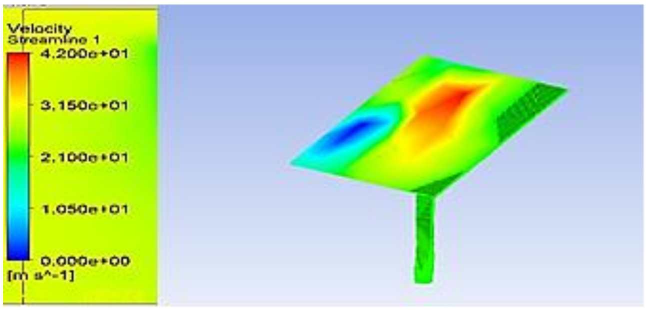

(c) H=3.35m

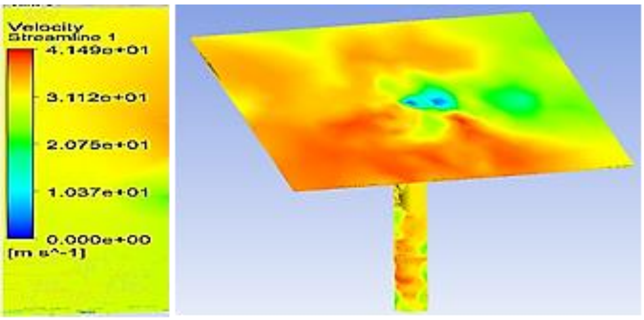

(d) H=3.35m

Fig 23. Velocity distribution of different heights of panel.

From a structural point of view, the stress values (Von Mises, normal, and the magnitudes of the shear) and deformation increased proportionally with the mounting height. This correlation is a direct consequence of the elevated aerodynamic forces acting on the system, which impose greater mechanical demands on the supporting structure.

Analyzing static structural contours at panel height of 2.5m, the total deformations, normal stresses, equivalent stresses, and shear stresses are again calculated. The resulting distributions are as illustrated in Fig. 24.

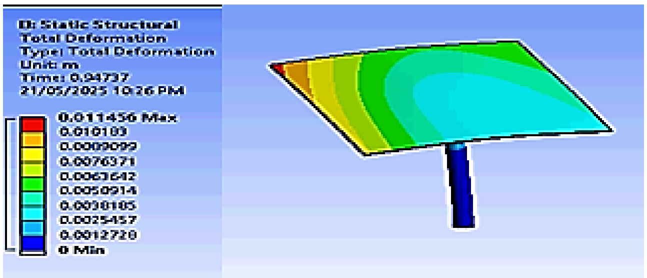

(a) total deformations

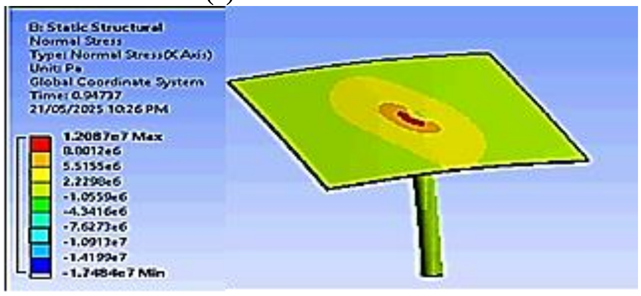

(b) normal stresses

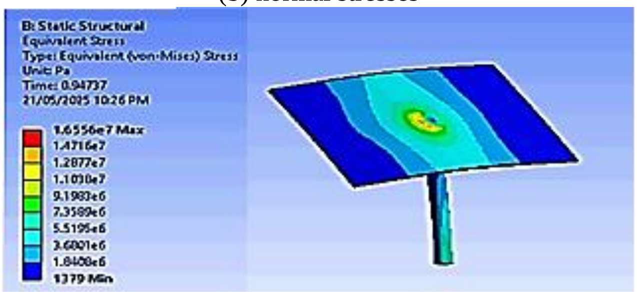

(c) equivalent stresses

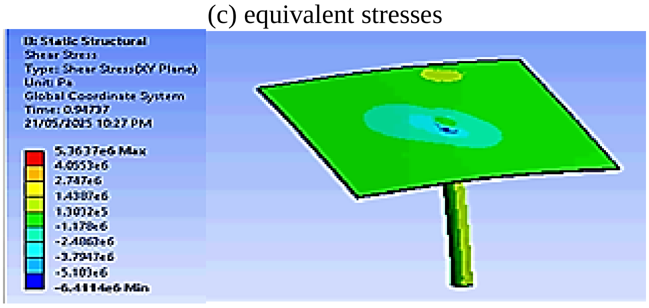

(d) shear stresses

Fig 24. Static structural contours at height of 2.5m.

D. *Effect of Panel Surface Area*

The CFD results demonstrated a clear trend. As the surface area increased, the magnitude of aerodynamic forces, namely, the drag force and lift force—also increased. This outcome is expected and logical, as aerodynamic forces scale proportionally with the exposed area facing the wind.

Furthermore, the drag coefficient (CD) showed a gradual increase with panel size, indicating a slight change in the flow behavior and an increase in overall resistance. The lift coefficient (CL) also exhibited a noticeable rise, reflecting the enhanced effect of vertical forces acting on a larger surface.

Fig. 25 illustrates the pressure distribution of panels with few distinct panel areas of 4.2×3.2m^2, 3×2m^2, 2×1m^2, and 1×0.7m^2.

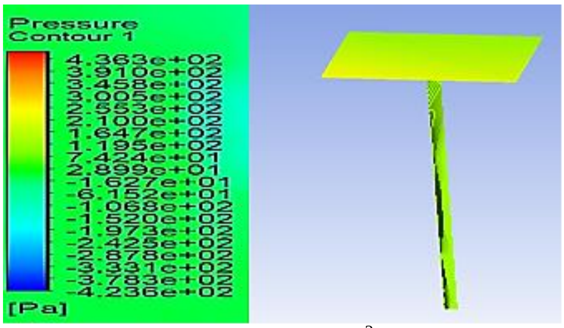

(a) A=4.2×3.2m^2

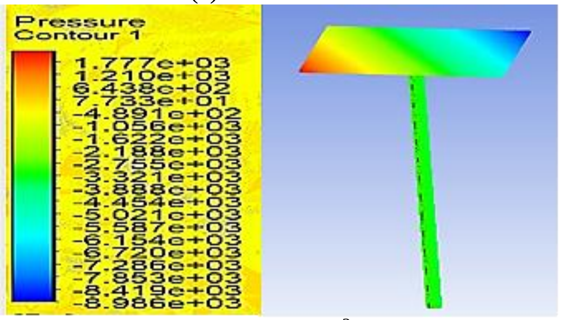

(b) A=3×2m^2

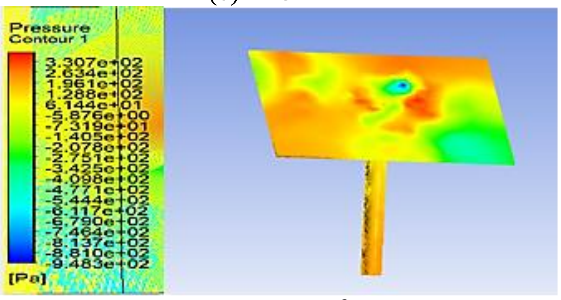

(c) A=2×1m^2

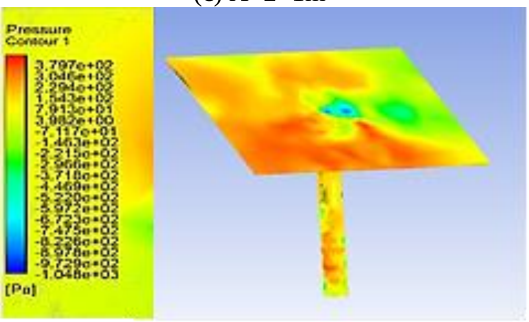

(d) A=1×0.7m^2

Fig 25. Pressure distribution in panels with few distinct areas.

Fig. 26 illustrates the velocity distribution of panels with the same panel areas of 4.2×3.2m^2, 3×2m^2, 2×1m^2, and 1×0.7m^2.

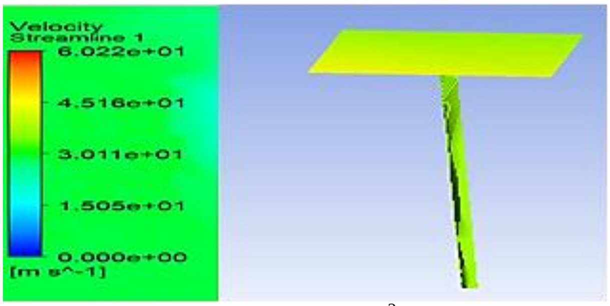

(a) A=4.2×3.2m^2

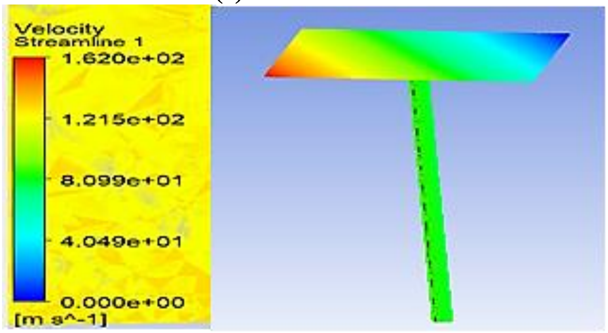

(b) A=3×2m^2

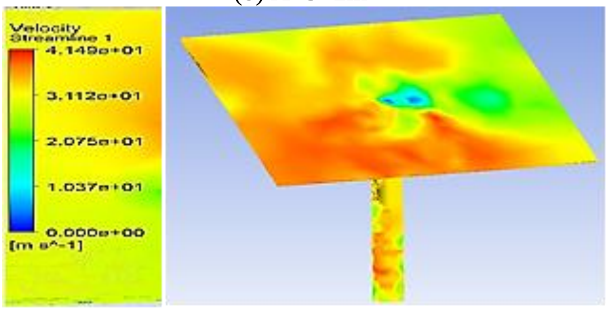

(c) A=2×1m^2

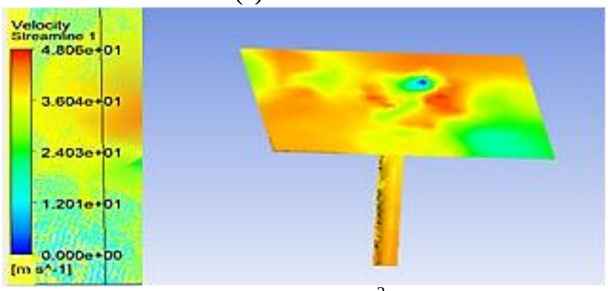

(d) A=1×0.7m^2

Fig 26. Velocity distribution in panels with different areas.

Structurally, the relationship between panel and stress levels was direct and significant. The largest panel (4.2×3.2 m) recorded the highest values for maximum total deformation, von Mises stress, normal stress and shear stress. This increase can be attributed to the combination of a stronger aerodynamic loading and a larger unsupported span, which makes the structure more susceptible to bending and deformation.

In contrast, smaller panels, particularly the 0.7×1 m configuration, demonstrated more stable structural behavior, with the lowest recorded values in all stress and deformation categories. This suggests a high structural resilience to wind loading, even without reinforcement.

Although smaller panels have proven to be structurally superior under wind loads, they are not necessarily the most practical or cost-effective option. Covering a given area with a high number of small panels may result in increased costs for support structures, cabling, and installation. Larger panels, on the other hand, offer better spatial efficiency and energy yield, but require a more robust structural design to withstand higher aerodynamic loads.

Therefore, a balanced recommendation would be to use medium-to-large panels (such as 2×3 m), which offer a good compromise between aerodynamic performance and structural safety. Additional reinforcement may be applied as needed to maintain structural integrity, especially in regions with high exposure to wind.

VII. Design Strategy: Numerical Experiments

To systematically investigate the effect of individual parameters on the aerodynamic and structural performance of solar panels, the numerical experiment design methodology was implemented. Specifically, the One-Factor-At-a-Time (OFAT) approach was adopted. In this strategy, only one variable is varied at a time, while all other parameters remain constant at their baseline values.

This method provides a clear and isolated understanding of the influence of each factor without introducing interactions between variables, which simplifies interpretation and improves the robustness of the conclusions. Although OFAT does not account for interaction effects between parameters, it is particularly suitable for computational studies where the cost of running simulations is high and isolating the contribution of each variable is essential. OFAT ensures reliable comparisons across different scenarios and builds a solid foundation for performance optimization under realistic environmental and design conditions. These aforementioned scenarios are summarized in Table 1. This strategic design choice strengthens the credibility of the simulation framework and aligns with established practices in computational experiment planning.

Table 1. Summary of the cases for parametric experimental design.

Experiment	Tilt angle (Deg)	Wind angle (Deg)	Area (m×m)	Height (m)
1	5	45	4.2*3.2	3.35
2	15	45	4.2*3.2	3.35
3	30	45	4.2*3.2	3.35
4	45	90	4.2*3.2	3.35
5	45	135	4.2*3.2	3.35
6	45	180	4.2*3.2	3.35
7	45	45	4.2*3.2	3.35
8	45	45	0.7*1	3.35
9	45	45	1*2	3.35
10	45	45	2*3	3.35
11	45	45	4.2*3.2	0.5
12	45	45	4.2*3.2	1.5
13	45	45	4.2*3.2	2.5

VIII. Conclusion

This current article successfully identifies optimal structural design strategies for PV solar panel mounting systems in wind-prone environments. The important conclusions withdrawn are the following:

- A tilt angle of 15° to 30° offers an optimal compromise between aerodynamic stability and structural performance.
- Mounting height between 1.5 m to 2.5 m provides good ventilation and limits excessive mechanical stress.
- Panels with moderate surface area such as 2×3 m are structurally safer while maintaining output efficiency.
- Structural reinforcement is necessary when using large panels or high tilt angles in exposed locations.
- Large tilt angles should be avoided in large open areas, unless additional reinforcement is provided.
- Site-specific wind analysis should be performed for better design outputs.
- Wind-induced vibrations imply the need for scheduled regular maintenance to avoid high stresses and probable fatigue problems.

References

[1] M. Shademan and H. Hangan, "Numerical simulation of wind loading on ground-mounted", NRC, rasearch press, 2014.

[2] M. Mohapatra, "Wind Tunnel Investigation of Wind Load on a Ground Mounted Photovoltaic Tracker", Colorado State University, CO, USA.," 2011.

[3] A. Darhouane, "Numerical investigation of wind load acting on a ground fixed solar panel", MSc thesis, 2022.

[4] A. Jubayer, K. Siddiqui, G. Bitsuamlak, and H. Hangan, "Numerical and experimental study of wind effects on photovoltaic (PV) panels", AAWE12 Workshop, Hyannis, MA, USA.2012.

[5] P. Kumar and S. B. Prakash, "CFD analysis of wind pressure over solar panels at different orientations of placement", International Journal of Advanced Technology in Engineering and Science, vol. 2 (7), pp. 313-320, 2014.

[6] O. Yemenici, "Aerodynamic Mechanisms on a Ground-Mounted", Uludağ University Journal of The Faculty of Engineering, 2020 .

[7] K. S. Apparao, "Structural orientation optimization of the pole mount support of a solar panel for wind load by using CFD analysis", International Journal of Advanced Research in Science and Technology, pp. 224-231, 2014.

[8] G. Baetu, C. Teleman, E. Axinte and V. Rosca, "Numerical Simulation of Wind Action on a Solar Panels Array for Different Wind Directions", Technical University of Iaşi, 2013.

[9] Hamza, Esam, et al. "CFD-Based Investigation of Flow Through an Orifice Plate Meter under Different Conditions." المجلة الليبية للدراسات الأكاديمية المعاصرة (2025): 245-258.

[10] Hamza, E. (2020). Dimensions Effect of the Rotating Fluid Zone on the Results when CFD Modelingof Friction Stir Welding. Third Conference for Engineering Sciences and Technology(CEST-2020). 01-03December 2020 /Alkhoms –Libya.

[11] Hamza, E. (2021). Cfd-modelling and thermal characterization of friction stir welding using tool with polygonal pins. J Eng Res, 32, 43-78.